The Biogenesis of Bacterial PHB Granules

Edward A. de Koning [a], Mayura Panjalingam [a], Jessica Tran [b], Michael R. Eckhart [b], Peter D. Dahlberg [c], Lucy Shapiro [a#]

[a]Department of Developmental Biology, Stanford University School of Medicine, Stanford, California, USA
[b]Stanford Protein and Nucleic Acid Facility, Stanford University School of Medicine, Stanford, California, USA
[c]Division of CryoEM and Bioimaging, SSRL, SLAC National Accelerator Laboratory, Menlo Park, California, USA.

Running Title: The Biogenesis of Bacterial PHB Granules

#Correspondence: shapiro@stanford.edu

Word count abstract: 189
Word count text: 5759

Abstract

PHB granules are bacterial organelles that store excess carbohydrates in the form of water-insoluble polyhydroxybutyrate (PHB). The biogenesis of these organelles has remained elusive. In this study, we show that PHB polymerase, phasin, and PHB synthesis are essential for PHB granule formation in *Caulobacter crescentus*. We show granule formation is initiated by the accumulation of PHB polymerase and subsequent recruitment of phasin. Phasin is a small amphipathic protein that is associated with PHB granules. Following the active synthesis of PHB, the polymerase dissociates from mature granules which coincides with recruitment of the PHB depolymerase. In the absence of phasin, PHB granules remain small and fail to increase past 250nm in diameter. The polymerase directly binds phasin *in vitro* through its intrinsically disordered N-terminal domain. Deletion of the polymerase N-terminus *in vivo* disrupts PHB granule formation and results in increased instability of the polymerase. Stability of the full-length polymerase is decreased under active PHB synthesis, potentially acting as a negative feedback loop on organelle biogenesis. Thus, the biogenesis of this membrane-less bacterial organelle uses an enzymatically active protein boundary to control the size and function of a carbon storage PHB granule.

Importance

Like Eukaryotes, bacteria organize their cytoplasm in subcellular compartments. These bacterial compartments can be membrane-bound (e.g. magnetosomes), protein-encased (e.g. carboxysomes), or membrane-less. Here we investigate how *Caulobacter* forms membrane-less compartments that store the water-insoluble carbohydrate polymer polyhydroxybutyrate (PHB). We find that PHB granules form by sequential recruitment of key proteins, and that the granule composition changes as these organelles mature. The PHB polymerase is essential for granule biogenesis and we describe a direct interaction with the granule associated protein phasin through the polymerase N-terminus. Deletion of this N-terminus limits granule formation and deletion of phasin halts granule maturation, resulting in smaller PHB granules. We propose a mechanism of granule formation that is regulated by PHB polymerase stability. Thus, granule biogenesis is initiated and controlled by the action of a PHB polymerase and an associated helper protein, phasin, that together synthesize the hydrophobic granule content while forming the granule's protein boundary.

Keywords: *Caulobacter*, bacterial organelle, PHB granule, PHB polymerase, phasin, PhaC PhaP, PhaR, PhaZ

Introduction

The compartmentalization of biochemical pathways in membrane bound subcellular organelles is commonly observed in eukaryotic cells. Although membrane bound compartments are not common in bacteria, there are instances of specific functions attributed to bacterial subcellular compartments such as membrane bound magnetosomes (1) and protein encapsulated carboxysomes (2) that sequester chemical processes. A third type of bacterial subcellular organelle, that is not membrane encapsulated, are those that store polyhydroxy butyrate, PHB (3). These granules are commonly found in many bacterial species, including *Caulobacter crescentus* (4). Consumption of PHB is increased under carbon starvation, suggesting that these granules function as carbohydrate storage organelles (5). Here, we have asked how a new organelle is formed and identified the steps required for the *de novo* formation of PHB granules in *Caulobacter crescentus*.

Polymers of PHB are hydrophobic and highly insoluble in water. Due to its hydrophobicity, accumulated PHB polymers could function as both the content of the organelle, and as its selective boundary. However, Cryo-EM images have shown that this boundary is composed of a discontinuous layer that is likely proteinaceous (6). Indeed, purified granules have been found to consist mainly of PHB (>95%) and associated proteins (7, 8) and are generally assumed to be membrane/lipid free (9). For an overview of PHB granule composition, see Figure 1A.

The most abundant granule associated protein is phasin (PhaP), a 15-25 kDa helix-turn-helix protein (10–12). Helical wheel predictions of phasin suggest that the protein is amphipathic, which would position the protein on the surface of the granule. It has been reported that phasin is localized to granule surfaces and can encapsulate purified PHB *in vitro* (10, 13, 14). The crystal structure of *Aeromonas hydrophila* phasin was recently solved revealing assemblies of phasins in stacked hairpins such that the hydrophobic surfaces are shielded from the solution, although it is not known if this conformation occurs *in vivo* on the surface of granules (15). A second protein predicted to reside on the granule surface is the PHB polymerase (PhaC) that catalyzes the polymerization of precursor monomers into PHB (16–18). The precursor monomer is generated in two steps from Acetyl-CoA by PhaA and PhaB to make (R)-3-hydroxybutanoyl-CoA (3HB-CoA) (Fig 1A) (16, 19, 20).

PHB is in a crystalline state when synthesized *in vitro*, chemically extracted from PHB containing bacteria, or found in the soil. In contrast, PHB in cells or in gently extracted

granules is amorphous (21–24). Bacterial PHB hydrolases can only degrade crystalline PHB (25). Amorphous PHB is specifically degraded by a depolymerase (PhaZ) (26), which is found associated with mature PHB granules (27, 28). The mechanism that keeps PHB in an amorphous state *in vivo* is unknown.

In this study we show that granule formation is dependent on the PHB polymerase PhaC, phasin PhaP and on the accumulation of the PHB polymer. Granules are formed *de novo* in *Caulobacter* by the initial sequestration of the PHB polymerase. Accumulation of the PHB polymerase is dependent on the intrinsically disordered N-terminus of the enzyme. The active polymerase catalyzes the accumulation of PHB from the 3HB-CoA precursor. Further accumulation of PHB is dependent on recruitment of phasin to the granule, potentially by the direct interaction of polymerase and phasin, which we have shown occurs *in vitro*. Granule synthesis is stopped by departure of polymerase from the newly formed granule, coincident with the recruitment of PhaZ depolymerase. Taken together, our observations describe a novel mechanism of granule biogenesis, where organelle initiation is dependent on an IDR region of a boundary protein that catalyzes the enzymatic reaction necessary to generate the hydrophobic content of the organelle, directly connecting the synthesis of both boundary and content.

Results

PHB granule formation requires both an active polymerase and phasin accumulation.

PHB synthesis is dependent on the acetyl-CoA acetyltransferase PhaA (CCNA_00544) and acetoacetyl-reductase PhaB (CCNA_00545) to produce the 3HB-CoA precursor from acetyl-CoA (20). These genes have not been previously described in *Caulobacter* but are annotated based on their homology. In *Caulobacter*, the polymerase PhaC (CCNA_01444) and the depolymerase PhaZ (CCNA_00250) have been described previously (4, 29). For an overview of PHB associated proteins, see Fig 1A. The only homologue to phasin found in *Caulobacter* is CCNA_02242, or PhaP from here on. To validate these candidates, we made use of hydrophobic dyes such as nile red and nile blue that have previously been reported to stain for PHB in a wide variety of bacteria (30–32). We observed fluorescent puncta in *Caulabacter* for both dyes, indicating the presence of PHB granules. These puncta were absent in a mutant lacking the polymerase *phaC* gene (Fig 1B). In cells where the transcription of *phaA* and *phaB* was controlled by a xylose inducible promotor, we could tune the amount of available precursor. By reducing the amount of PhaA and PhaB expression we observed a clear

reduction in nile blue signal (Fig. 1C). This indicates that not just the presence, but the activity of the PhaC polymerase is necessary for the nile blue puncta. Deleting phasin also affects puncta formation, as it reduces the number of puncta by 90% (Fig. 1D). Deletion of the depolymerase did not affect the number of puncta per cell (Fig. 1B).

Polymerase accumulation initiates granule biogenesis

The different mutant strains were also imaged using cryo EM. This confirmed the absence of any PHB granules in the Δ*polymerase* mutant, but it revealed many small PHB granules in the Δ*phasin* mutant (Fig. S1). These small granules were likely below the detection limit using the nile red stain (Fig. 1) and could point to an arrested growth of PHB granules in the absence of phasin. To study time dependent granule biogenesis, we first starved cells for glucose for at least 24hrs, which resulted in a complete lack of nile red stained granules, presumably due to the consumption of all PHB. Reintroducing glucose in the medium restored nile red-stained granules within 2 hours (not shown), providing a window of time to study *de novo* granule formation. Using timelapse microscopy, we followed polymerase-GFP and phasin-mCherry signal as starved cells were allowed to recover on glucose containing agarose pads. In starved cells, the polymerase signal was observed to be mostly diffuse with a few puncta, while the phasin signal was diffuse (Fig. 2A or B, t=0). The condensation of polymerase is the first event in granule biogenesis, as the polymerase-GFP signal condensed into clearly delineated puncta, while only a small portion of the diffuse phasin began to colocalize with the polymerase (Fig. 2A, compare t = 0 to t=45 min). Only after the polymerase formed distinct foci did we observe the remaining phasin cleanly accumulate into these puncta (Fig. 2A, compare t = 45 to t=135). Finally, the polymerase signal decreased, leaving behind just the phasin signal (Fig. 2A, t=180). New polymerase puncta were observed that repeated the process (Fig. S2).

The departure of the polymerase from a newly formed granule appears to coincide with the mature granule's final size. We asked if this departure coincided with the recruitment of the depolymerase, which is necessary for granule consumption. In recovering cells, upon the addition of glucose at time 0, polymerase-GFP puncta were observed, but no depolymerase-mCherry signal (Fig. 2B, t=0). Depolymerase-mCherry arrived at the puncta as polymerase-GFP left (Fig. 2B, t=120). These results demonstrate that PHB granule composition changes over time, initiated with polymerase localization, followed by phasin accumulation and finally by the recruitment of the depolymerase and loss of polymerase in older granules.

We used correlative light and electron microscopy (33–35) with cells expressing GFP-tagged PHB polymerase to image PHB granules (Fig 3A). We detected small granules that contained polymerase-GFP and larger PHB granules that exhibited both polymerase and PHB, confirming the order of granule assembly observed in the time lapse images shown in Fig 2. It should be noted that a small amount of newly synthesized PHB is likely present in the early small granules that is below the detection of Nile Red staining, because PHB may start accumulating as soon as polymerase condenses into a nascent granule. There is a size dependent correlation between the Nile Red intensity and the granule diameter (Fig S1). The accumulation of the polymerase to initiate nascent granule formation may be enhanced by polymerase self-interaction. Using surface plasmon resonance, purified PHB polymerase was tested for its ability to self-interact (Fig. 3B left panel). A strong response is observed when increasing concentrations of polymerase are flown over surface-immobilized polymerase, indicating a strong self-interaction of the PHB polymerase.

The polymerase unstructured N-terminus binds phasin and protects the polymerase against PHB-synthesis induced instability.

We have observed that polymerase localization in puncta and subsequent phasin accumulation are both required for mature granule formation. Additionally, precursor production is required for nile red accumulation (Fig 1), while the majority of granules in a phasin mutant do not stain for nile red, fail to reach maturity and do not expand in size past 250 nm in diameter (Fig. S1). This suggests that active polymerase promotes phasin accumulation, which in turn reinforces polymerase activity. To explain this self-reinforcing loop, we studied a potential interaction between polymerase and phasin.

Using bacterial two-hybrid (BACTH), we show that phasin and polymerase both self-interact, and interact with each other when co-expressed in *E. coli* (Fig. S3A). Using purified *Caulobacter* polymerase and phasin proteins, we assayed the polymerase/phasin interaction *in vitro* using surface plasmon resonance (SPR, Fig. 4A). With phasin immobilized on the surface, we observe a polymerase concentration-dependent response in signal (Fig. 4A, top graph). This binding was observed irrespective of which protein was immobilized on the surface (Fig. S3B). This direct interaction was surprising, since phasins in two other bacterial species do not directly bind the polymerase when tested by BACTH or crosslink pull-down (36, 37). The *Caulobacter* polymerase has an N-terminal, intrinsically disordered domain that is

not present in polymerase from either one of the two bacteria examined, *P. putida* or *C. necator* polymerase (38). Repeating the SPR with purified, N-terminally truncated polymerase (polymeraseΔN) resulted in a complete lack of binding with phasin (Fig. 4A bottom panel). However, polymeraseΔN was still able to interact with full-length polymerase (Fig. 3B right panel).

To study the effect of disrupting the polymerase-phasin interaction *in vivo*, a mutant strain lacking this unstructured N-terminus was created. PolymeraseΔN cells, where the PolymeraseΔN-GFP was the only PHB polymerase in the cell, exhibited a complete lack of nile blue stained granules, and polymeraseΔN-GFP failed to accumulate into defined puncta in this mutant strain (Fig. 4B), even though PolymeraseΔN can self-associate (See Fig 3B right panel). This suggests that the N-terminus or another factor, possibly phasin, enables defined granule formation. Cryo-EM images of the polymeraseΔN strain showed a reduction in granules like that observed in a Δpolymerase strain (Fig. S4), with the very few granules present in the mutant cells having a diameter below 250nm. Since the polymeraseΔN mutant phenocopies the Δpolymerase mutant, we asked if the *polymeraseΔN* allele was still transcribed. Using primers against the 3' end of *phaC*, the transcription of *polymerase* (*phaC,* CCNA_01444) and *polymeraseΔN* were tested by qPCR (Fig. 4C). As expected, *phaC* transcription was not detected in the Δ*polymerase* mutant. Deleting the 5' part of *phaC* led to a 60% reduction in transcription of *polymeraseΔN* in cells where *polymeraseΔN-gfp* is the only *phaC* allele present. Transcription of *phaC* was not altered in a Δ*phasin* strain, despite the reduction in PHB granule sizes observed in this mutant background (Fig. S1).

To determine if there was an effect on *phasin* transcription in the polymeraseΔN mutant strain, the transcription of *phasin* (*phaP,* CCNA_02242) in different mutant backgrounds was quantified using qPCR (Fig. 4C). As expected, *phasin* transcription was not detected in a Δ*phasin* mutant. However, in both the Δ*polymerase* and *polymeraseΔN* mutant backgrounds *phasin* transcription was reduced by over 90% (Fig. 4C). Δ*CCNA-00543* is a candidate for the *Caulobacter* gene encoding the PhaR repressor of *phasin* transcription observed in other bacterial species (39–42). We observed that *phasin* expression was increased by 6-fold in the Δ*CCNA_00543*, confirming this as the repressor (PhaR) in *Caulobacter* (Fig 4C). PhaR repression has been proposed to be relieved by sequestration of PhaR to the PHB granule (42, 43). Therefore, the inability of the Δ*polymerase* and *polymeraseΔN* mutants to make PHB granules could in turn explain the low *phasin* transcription observed in these backgrounds.

PhaR has not been reported to affect *phaC* transcription, and we observe similar *polymerase* transcription in the Δ*CCNA_00543* background compared to WT (Fig. 4C).

To compensate for the reduction in *polymeraseΔN* transcription compared WT *polymerase* transcription, we expressed either full-length polymerase-FLAG or polymeraseΔN-FLAG from the *xylX* locus as the only polymerase copy. The expression of these proteins was compared to polymerase-FLAG and polymeraseΔN-FLAG expressed from their native locus by western blot using anti-FLAG antibody. At 0.01% xylose induction, the full-length polymerase expression was comparable to the native expression of polymerase-FLAG, with clear over-expression at 0.1% xylose induction (Fig. S5). However, no polymeraseΔN-FLAG signal was detected, even when expressed at 0.1% xylose induction.

The loss of polymeraseΔN-FLAG could indicate degradation or instability of the protein. Deletion of the N-terminus of the *Caulobacter* PHB polymerase has previously been reported to reduce its catalytic rate by up to 50 fold (38, 44). To study if this reduction of catalytic activity causes the reduction in polymeraseΔN levels, polymerase and polymeraseΔN expression was tested under conditions that reduce PHB synthesis. Deleting *phaAB* abolishes precursor production and thus PHB synthesis, and additional deletion of the repressor *phaR* ensures the expression of PHB related proteins independent of the presence of PHB. Surprisingly, deleting precursor production increased polymerase and polymeraseΔN protein levels (Fig. 4D). Directly inactivating polymerase activity by mutating the active site cysteine to an alanine (C406A) also further stabilized full length polymerase, but this did not stabilize polymeraseΔN (Fig. S7A). Since deletion of the repressor *phaR* leads to an increase in *phasin* transcription (Fig 4C), we tested if the lack of PhaR could be contributing to the increased stability of polymeraseΔN in the Δ*phaRAB* background. However, over-expression of phasin did not further stabilize polymeraseΔN (Fig. S7B). Together, these results indicate that active synthesis of PHB destabilizes the polymerase, and that the N-terminus protects the polymerase against this instability.

Discussion

In this study, we asked how *Caulobacter* forms PHB granules *de novo*. We show that the combined action of the PHB polymerase (PhaC) and phasin (PhaP) that carry out the synthesis of PHB, are essential for PHB granule formation. We found that localized accumulation of polymerase initiates granule formation, while subsequent accumulation of phasin is required

to increase PHB granules to its mature size. The unique unstructured N-terminus of the *Caulobacter* PHB polymerase directly binds phasin and is required for *in vivo* stability of the polymerase. Polymerase stability is increased by inactivation of PHB synthesis suggesting a model of granule formation in which PHB negatively regulates its own synthesis by inactivation of the polymerase through protein instability.

The sequential localization of granule associated proteins illustrates that the composition of individual PHB granules changes over time, similar to changes in the composition of magnetosomes and carboxysomes during their formation (1, 2, 45). Magnetosomes are membrane bound organelles in which magnetite is stored, enabling their magnetotactic bacterial hosts to orient themselves within a magnetic field, assisting in chemotaxis (1, 46, 47). During magnetosome biogenesis, the bacterial inner membrane invaginates to form a compartment, followed by the accumulation of magnetite (1, 48, 49). Carboxysomes, which carry out carbon fixation and are responsible for efficient photosynthesis under low CO_2 concentrations, are not encapsulated by a membrane. The key photosynthetic protein, RuBisCo, is first condensed into a pre-carboxysome. Shell proteins are then recruited to encapsulate this condensate generating a finished carboxysome (2, 50). PHB granules are not membrane bound, but there is also no evidence of a continuous protein shell (6, 9). As active PHB synthesis is required for granule formation, PHB 'seeds' emerging from the polymerase prior to granule formation could help drive initial accumulation. Considering PHB is highly water insoluble, phase transition could function as a selective barrier for this organelle. This interface between cytoplasm and PHB is the most likely site for accumulation of granule associated proteins. Since PHB synthesis is required for granule formation, the volume to surface ratio changes as a granule increases in size. This ratio could play a role for selective protein recruitment to the granule surface.

The recruitment of depolymerase (PhaZ) following that of the polymerase answers a previous paradox of futile PHB cycling (51, 52). Studies observed the expression of both PHB polymerase and depolymerase in cell cultures, suggesting that PHB is both formed and consumed (53, 54). Purified granule populations also show the presence of both polymerase and depolymerase (8). However, in both cases an ensemble measurement was made. In our single cell imaging experiments, we observed that while PHB polymerase and depolymerase can be expressed in the same cell, at any given time they are present on different PHB granules (Fig 2).

Phasin isolated from *Pseudomonas putida* has been shown to encapsulate PHB *in vitro* (14), and, *in vivo*, phasin protein levels were found to increase during PHB production *C. necator* and *Caulobacter* (40, 44). *In vitro* reactions of PHB synthesis occur in cm sized aggregates indicating the tendency of PHB to self-associate (55). Further, a previous cryo-EM study suggested that the bimodal distribution of granules size might indicate granule fusion *in vivo* (6). Thus, it is possible that PHB granules fuse and that this fusing is coordinated by phasin, although granule fusion has so far not been observed directly. Deletion of *Caulobacter* phasin disrupts the formation of mature granules, and instead leads to the accumulation of small immature granules (Fig. S1). Because of the observed sequential recruitment of polymerase and phasin (Fig 2), the smaller size of PHB granules in a *phasin* mutant could indicate a premature departure of polymerase from this granule. Thus, changes in the number and size of granules likely reflect differences in the rate of granule initiation, granule growth, and departure of polymerase from existing granules.

Strong polymerase self-interaction, measured by SPR (Fig 3B), likely contributes to its localized accumulation and the initiation of granule formation. Since PHB synthesis is required for granule formation (Fig 1), cells can control granule formation by directly controlling polymerase activity. Phosphorylation of the polymerase has been reported to control PHB synthesis in *C. necator* (56). However, the reported phosphorylated threonine residue (T373) is not conserved in *Caulobacter.* Here, we find that in *Caulobacter* it is the stability of the polymerase that is regulated. Polymerase stability is improved in cells that do not make any PHB, suggesting a negative feedback loop of PHB on the polymerase.

The polymerase N-terminus directly binds phasin, recruiting it to the PHB granule. It also protects the polymerase against degradation, as seen by the increased instability in a N-terminal mutant (Fig 4). The intrinsically disordered N-terminal extension of the polymerase is unique to *Caulobacter*, but it shows sequence and functional homology to PhaM in *C. necator*. PhaM contains an intrinsically disordered region comprised of lysine, proline, and alanine repeats (57), which is also found in the *Caulobacter* polymerase N-terminus. The N-terminal mutant of *Caulobacter* polymerase shows a lag in *in vitro* PHB synthesis (38), like that observed for *C. necator* polymerase (38). Addition of PhaM to the *C. necator* polymerase was reported to overcome this initial lag phase (58), like the absence of lag phase reported for the full length *Caulobacter* polymerase (38). PhaM has been shown to associate with PHB granules, and in mutants lacking PhaM fewer PHB granules are observed (3, 59). Thus, the intrinsically disordered N-terminus of the *Caulobacter* polymerase functions in a manner

analogous to the disordered *C. necator* PhaM protein and underscores a role for the N-terminal region of the *Caulobacter* polymerase in the initiation of granule biogenesis, possibly due localized phase transition initiated by the polymerase self-interaction and the N-terminal intrinsically disordered region, or by recruitment of the phasin necessary for granule formation.

PHB granule formation appears to be highly regulated and intricately linked to central carbon metabolism in *Caulobacter*. Precursor synthesis from acetyl-CoA directly links granule formation and growth to the metabolic state of the cell, possibly functioning as an overflow metabolite. If there is no need to make PHB, no organelle will be formed. Phasin is essential for the continued growth of the PHB granule, and regulation of its expression by the repressor PhaR ensures that it is only expressed if PHB is synthesized. Both phasin recruitment and polymerase stability are controlled by the N-terminus of the polymerase, and both are required for PHB granule formation. As part of the organelle boundary, this all puts the PHB polymerase at the center of organelle formation; ensuring that its enzymatic activity continues at the granule surface directly dictates PHB granule formation and growth. Inactivation of the polymerase by direct degradation or limiting precursor abundance allows the cell to control how large a PHB granule grows, or if new granules should be formed.

Investigating the formation of PHB granules provides insight into the biogenesis of bacterial organelles, and comparing PHB granule formation to carboxysome and magnetosome formation highlights shared themes (i.e. sequential recruitment of key proteins) and differing solutions to similar challenges (i.e. the establishment of the border between organelle content and the surrounding cytoplasmic environment).

Material and Methods

Bacterial growth conditions

Unless stated otherwise *Caulobacter* strains were inoculated from glycerol stock in PYE for overnight growth at 30°C under aeration. Antibiotics were used for selection during strain construction and added for selective pressure for single-crossover integrated constructs. Antibiotic concentrations that were used (liquid/solid): spectinomycin (25/50 µg/ml), kanamycin (5/25 µg/ml), rifampicin (2.5/5 µg/ml), gentamicin (0.5/5 µg/ml), tetracycline (1/1 µg/ml) and chloramphenicol (2/1 µg/ml). *Escherichia coli* strains were inoculated from glycerol stock in LB for overnight growth at 37°C under aeration. The following concentrations of antibiotics were used for *E. coli*: spectinomycin (50/100 µg/ml), kanamycin (50/50 µg/ml),

rifampicin (25/50 μg/ml), gentamicin (15/20 μg/ml), tetracycline (12/12 μg/ml) and chloramphenicol (20/30 μg/ml). All strains used in this study are listed in table S1.

Plasmid and strain construction

Plasmids were constructed using previously reported plasmids (60). Plasmids used in this study were either; i) ordered from Synbio Technologies, ii) constructed using Gibson Assembly (GA) protocol from New England Biolabs (NEB) or iii) using restriction-ligation per NEB protocol. Plasmids and primers used in this study are listed in table S2. Plasmids were isolated using Monarch Plasmid Miniprep kit from NEB and linearized using restriction enzyme by NEB as per manufacturer's protocol. Inserts were acquired by PCR using KOD Hotstart Mastermix from NovaGen and purified from gel using Monarch DNA Gel Extraction kit from NEB. All cloning was performed in *E. coli* using ultracompetent DH5α from NEB by heat shock as per manufacturer's protocol. Plasmids were transformed to *Caulobacter* by electroporation. For marker-free integration and deletion, plasmids were first integrated selecting for kanamycin resistance, after which counter-selection on sucrose was performed (60). Kanamycin sensitive candidates were verified by PCR.

pEK001 was constructed by 2 fragment GA using pET28a linearized with BamHI and NheI as backbone and CCNA_01444 amplified from gDNA with EKP001 and EKP002 as insert. pEK003 was constructed by 4 fragment GA using pNTPS138 linearized by HindIII and NheI, *CCNA_02242* CDS without stop codon including 368bp upstream amplified from gDNA genomic DNA (gDNA) with EKP005 and EKP006, mCherry amplified from pCHYC-1 with EKP007 and EKP008, and 800bp downstream of *CCNA_02242* amplified from gDNA with EKP009 and EKP010. pEK005 was constructed by Synbio using PCR cloning, combining synthesized *CCNA_01444* 3' 800bp into pGFPC-4 backbone. pEK011 was constructed by Synbio using gene synthesis using pET28a as a backbone and *CCNA_02242* as synthesized insert. pEK012 was constructed by Synbio using gene synthesis, combining the fragments 800bp upstream *CCNA_02242*, the chloramphenicol cassette from pMCS-6, and 800bp downstream of *CCNA_02242* into pNPTS138. pEK013 was constructed by Synbio using gene synthesis, combining 800bp upstream of *CCNA_00250*, the tetracycline cassette from pMCS-5, and 800bp downstream of *CCNA_00250* into pNPTS138. pEK014 was constructed by Synbio using gene synthesis, combing 800bp upstream of *CCNA_01444*, the rifampicin cassette from pMCS-3, and 800bp downstream of *CCNA_01444* into pNPTS138. pEK022 was constructed by 2 fragment GA using backbone pXMCS-2 linearized with KpnI and NdeI and insert 5' 800bp of *CCNA_00544* amplified with EKP015 and EKP016 from gDNA. pEK026-pEK033 were all made using restriction ligation, using XbaI and EcoRI linearized backbones and for the inserts

forward primers introducing XbaI and reverse primers EcoRI. CCNA_02242 was amplified with EKP032 and EKP033 from gDNA and ligated into pKT25 (pEK026) and pUT18C (pEK027) for N-terminal fusions. CCNA_02242 was amplified with EKP036 and EKP037 from gDNA and ligated into pKTN25 (pEK030) and pUT18 (pEK031) for C-terminal fusions. CCNA_01444 was amplified with EKP034 and EKP035 from gDNA and ligated into pUT18C (pEK029) for N-terminal fusion. CCNA_01444 was amplified with EKP038 and EKP039 and ligated into pKTN25 (pEK032) and pUT18 (pEK033) for C-terminal fusions. pEK035 was constructed by amplifying pEK001 using EKP040 and EKP041, digesting the PCR product with NheI and ligating the ends back together. pEK036 was constructed by 3 fragment GA using as backbone pEK014 amplified with EKP043 and EKP044, CCNA_01444 256-2016bp amplified with EKP045 and EKP046 from gDNA, and GFP amplified with EKP047 and EKP048 from pEK005. pEK039 was constructed by 3 fragment GA, using pNPTS138 linearized by HindIII and NheI as backbone, 800 bp downstream of CCNA_00543 amplified with EKP053 and EKP054 from gDNA, and 800bp upstream of CCNA_00543 amplified with EKP055 and EKP056 from gDNA. pEK043 was constructed by 3 fragment GA, using pNPTS138 linearized by HindIII and NheI as backbone, 1000bp downstream of CCNA_00543 amplified with EKP053 and EKP061 from gDNA, and 1000bp downstream of CCNA_00545 amplified with EKP062 and EKP063 from gDNA. pEK044 was constructed by 4 fragment GA, using pNPTS138 linearized with HindIII and NheI as backbone, 3’ 800bp of CCNA_00250 amplified with MP001F and MP002R from gDNA, mCherry amplified from pCHYC-1 with MP002F and MP002R, and 800bp downstream of CCNA_00250 amplified with MP003F and MP003R from gDNA. pEK047 was constructed by 2 fragment GA replacing the GFP of pEK036 with a 1x FLAG tag, PCR product 1 was pEK036 amplified with EKP045 and EKP069 and PCR product 2 was pEK036 amplified with EKP044 and EKP070. pEK050 was constructed by 2 fragment GA, using pTC88 linearized with KpnI and NdeI as backbone, and CCNA_01444 amplified with EKP075 and EKP076 from gDNA as insert. pEK051 was constructed by 2 fragment GA, using pEK047 linearized by KpnI and EcoR1 as backbone, and 3xFLAG linker amplified from pTC88 with EKP077 and EKP078 as insert. pEK052 was constructed by 2 fragment GA, using pTC127 linearized by NdeI and SacI as a backbone, and CCNA_01444 amplified from gDNA with EKP083 and EKP084 as insert. pEK053 was constructed by 2 fragment GA, using pTC127 linearized by NdeI and SacI as backbone, and CCNA_01444 256-1761bp amplified from gDNA with EKP083 and EKP085 as insert. pEK054 was constructed by 3 fragment GA, using pTC127 linearized by NdeI and SacI as backbone, CCNA_01444 1-1215bp amplified from gDNA with EKP084 and EKP087, and CCNA_01444 1217-2019bp amplified from gDNA with EKP083 and EKP086. pEK055 was constructed by 2 fragment GA, using pXCHYC-2 linearized with NdeI and NheI as backbone, and CCNA_02242

amplified from gDNA with EKP071 and EKP074 as insert. pEK056 was constructed by 3 fragment GA, using pTC127 linearized by NdeI and SacI as backbone, and CCNA_01444 256-1215bp amplified from gDNA with EKP085 and EKP087, and CCNA_01444 1217-2016bp amplified from gDNA with EKP083 and EKP086.

Staining of PHB granules

Caulobacter cells were inoculated from glycerol stock into PYE and grown overnight at 30°C. Overnight cultures were subcultured in M2G minimal media and grown overnight at 30°C. For nile red staining, cells were washed in PBS and stained in PBS and 1μM nile red (final concentration) for 20 minutes at room temperature. Cells were washed in PBS and subsequently imaged. For nile blue staining, 10μM nile blue (final concentration) was added directly to the media and cells were stained for 20 minutes at room temperature. Cells were washed in M2G and subsequently imaged.

Room-temperature fluorescent microscopy and image analysis

Unless otherwise stated, cells were imaged on M2G 1% agarose pads on a Leica Dmi8 multicolor epifluorescence microscope. A phase-contrast 100x oil immersion objective was used with a Lumencor SpectraX LED light source. Images were captured on an EMCCD camera (Hamamatsu C9100 02 CL). GFP was imaged at 480nm excitation and 527nm emission. mCherry, nile red and PHB specific nile blue were imaged at 554nm excitation and 609nm emission. Nile blue membrane stain was imaged at 635nm excitation and 680nm emission. Images were analyzed and quantified using ImageJ (Fiji).

Cryogenic electron microscopy

Single cryogenic transmission electron micrographs of *C. crescentus* were acquired using a 300 keV electron microscope (G3 Titan Krios™) equipped with direct electron detection camera with a BioQuantum™ Imaging Filter (Gatan, Inc) using a 30-eV slit width. The effective pixel size was ~6.5 Å, target defocus was 10 μm and the total dose was 25 $e^-/Å^2$. For presentation the data was binned by 4 into 2.6 nm pixels. Acquisitions were controlled using SerialEM software (61).

Cryogenic correlative light and electron tomography

Cryogenic light microscopy for correlative imaging was acquired on a home-built light microscope (62). Light microscopy was performed using either 488 nm (imaging of GFP channel) or 561 nm (imaging of nile red channel) laser-based illumination through a 100x

objective (Nikon CFI TU Plan Apo 100x/NA0.9). Intensities at the sample were kept below 50 W/cm^2 to avoid sample heating and devitrification(63). Fluorescent emission was detected with an EMCCD camera (Andor iXon) after passing through a 488 nm and 561 nm notch blocking filters and either a 525/50 bandpass for the GFP channel or 607/70 bandpass filter for the nile red channel. Despite both color channels being collected on the same detector, slight shifts in the relative position of the images were corrected for by translating one color channel to align common features, such as grid holes, for each field of view. The excitation beam profiles were measured using a thin film of fluorescent dye embedded in PVA-VA spun on a coverslip. Fluorescent brightness across the field of view was corrected for by dividing acquired images by a Gaussian fit to the measured beam profiles.

Subsequent electron tomography was performed on a 300 keV electron microscope (G3 Titan Krios™) equipped with direct electron detection camera with a BioQuantum™ Imaging Filter (Gatan, Inc) using a 20-eV slit width. The effective pixel size was 4.49 Ångstroms. The tilt series was acquired unidirectionally over ±46 degrees in 2 degree steps. Total dose was 100 $e^-/Å^2$. Reconstructions were performed using IMOD with data binned-by-4 to produce 1.8 nm effective pixels (64). Registration of light microscopy and electron tomography datasets was performed using a projective transformation first to a lower magnification cryoEM micrograph and then a similar transformation to the higher magnification tomography datasets. Further details on the registration process can be found in Dahlberg et al (35).

Timelapse microscopy

Overnight PYE cultures of *Caulobacter* were subcultured in M2G minimal media and grown at 30°C overnight. The culture was washed in M2 and resuspended in M2 and starved 24 hours at 30°C. Just prior to imaging, cells were pelleted and resuspended in M2G and spotted on M2G pads. The coverslip was sealed by wax to prevent evaporation and the recovering cells were imaged at 15-minute intervals for at least 3 hours.

Protein interaction by bacterial-two-hybrid

E. coli BTH101 was grown overnight in LB and washed in MQ. Washed cells were transformed with 1µl T18 expressing plasmid and 1µl T25 expressing plasmid by electroporation (1.67V, 400 Ohm). After recovery, transformants containing both plasmids were selected on LB plates containing both kanamycin and ampicillin. These candidates were streaked onto MacConkey agar plates (4% MacConkey agar, 1% maltose, 100µg/ml ampicillin, 50µg/ml kanamycin, 1mM IPTG) and grown at 37°C. A positive interaction was indicated by a purple color, while white/transparent streaks were considered absence of interaction.

Protein purification

His-tagged proteins were expressed in *E. coli* BL21(DE3) using the pET28a system. Cells were grown overnight at 37°C in LB and diluted 1:400 into prewarmed LB. At an OD_{600} of approximately 0.5, protein expression was induced with 0.4μM IPTG and the culture was shifted to 18°C for another 3 hours. Cells were washed in ice-cold PBS and the pellet was stored at -80°C. Cells were thawed on ice and resuspended in ice-cold lysis buffer (50mM HEPES-KOH pH 8.0, 500mM KCl, 25mM imidazole, 1 protease tablet per 50mL buffer, 200U benzonase nuclease at 0.3ul per 1L culture). Cells were lysed by sonication (3 sec pulse, 12 sec rest, 100% amplitude, 4 minute total pulse) and the lysate was cleared by centrifugation (30 minutes, 4°C at 29000 rcf). Cleared lysate was inoculated with pre-equilibrated Ni-NTA resin (1ml per 1l culture) for 2 hours at 4°C under gentle agitation. The lysate-resin mixture was separated by a gravity column (Poly-Prep Chromatography Column, Bio-Rad) and the resin was washed with 15 column volumes (CV) wash buffer (50mM HEPES-KOH pH 8.0, 500mM KCl, 25mM imidazole). The sample was eluted in 5 CV elution buffer (50mM HEPES-KOH pH 8.0, 500mM KCl, 250mM imidazole, 10% glycerol) and stored at -80°C. For the removal of the His6-tag, a Thrombin CleanCleave Kit (Sigma) was used.

Surface Plasmon Resonance

Reagents: Sensor CM5 chips, N-Hydroxysuccinimide (NHS), 1-Ethyl-3-(3-dimethylaminopropyl) carbodiimide (EDC), and ethanolamine hydrochloride (EA) were obtained from GE Healthcare/Cytiva. Surface Plasmon Resonance experiments were performed on a BIACORE 3000 biosensor system (GE Healthcare/Cytiva) at 25ºC. Proteins were dialyzed against Assay Buffer (20mM HEPES pH7.4, 200mM NaCl) before use. The different proteins (His-tagged or untagged Polymerase (PhaC) and phasin (PhaP)) were covalently immobilized on the surface of a CM5 biosensor chip (GE Healthcare/Cytiva) by amine coupling chemistry using N-hydroxysuccinimide (NHS) and N'-(3-dimethylaminopropyl) carbodiimide hydrochloride (EDC) according to the manufacturer's instructions. To investigate binding of Polymerase (PhaC) or phasin (PhaP) to the immobilized Polymerase (PhaC) or phasin (PhaP), dialyzed proteins were diluted in Assay Buffer and injected over the Ligand containing surface for 2min at different concentrations at a flow rate of 30 μl/min. For each experiment at least 5 different concentrations of analyte proteins were injected over each experimental and control flow cell. Dissociation was allowed to occur at the same flow rate for 300 sec. followed by Regeneration Buffer (20mM HEPES pH7.4, 1M NaCl) at a flow rate of 100 μl/min for 30sec and Assay Buffer alone at a flow rate of 30 μl/min

to allow the baseline to stabilize. All data were corrected for unspecific binding by subtracting the signal measured in a control cell lacking immobilized ligand. Data analysis was performed using the BIAevaluation software 4.1 (GE Healthcare/Cytiva).

qPCR

Overnight cultures of *Caulobacter* were diluted 200x into M2G minimal media and grown for 16 hours at 30°C. Samples were collected and RNA was extracted using RNeasy Protect Bacteria Mini Kit (Qiagen) per manufacturer's protocol. The quality and amount of RNA collected was analyzed using NanoDrop and sample concentrations were adjusted for cDNA synthesis using Superscript III (Invitrogen) per manufacturer's protocol. qPCR was performed on cDNA using FastSYBR Green Master Mix (Applied Biosystems) per manufacturer's protocol. The primers that were used are listed in Table S2C. The resulting amplification curves were analyzed using Desing & Analysis 2.6.0 (Applied Biosystems) and with the resulting threshold cycles the fold change was calculated using ΔΔCt method (65).

Western Blot

Overnight cultures of *Caulobacter* were diluted 200x into M2G minimal media and grown overnight at 30°C. Cells were collected and samples were normalized by OD_{600}. Samples were analyzed by Western Blot as described previously (66).

Acknowledgements: We thank T. Chong for providing plasmids and thank T. Chong and S. Saurabh for helpful discussions on experimental aspects of the manuscript. We thank all members of the Shapiro laboratory for constructive feedback throughout this work. **Funding:** This work was supported by the National Institutes of Health (R35-GM118071 to L.S). L.S. is a Chan Zuckerberg Biohub Investigator. P.D.D. was supported in part by the Panofsky Fellowship at the SLAC National Accelerator Laboratory as part of the Department of Energy Laboratory Directed Research and Development program under contract DE-AC02-76SF00515 and by grant 2021-234593 from the Chan Zuckerberg Initiative DAF, an advised fund of Silicon Valley Community Foundation. **Author contributions:** This study was conceived by E.A.K. Experiments were designed by E.A.K., with input from L.S., M.E. and P.D.D. Strains for this study were engineered by E.A.K. and M.P. Room temperature fluorescent microscopy, Western Blot and qPCR were performed by E.A.K. and M.P and analyzed by E.A.K. Protein purification and BACTH were done by E.A.K. SPR was performed by J.T. and M.R.E. and analyzed by M.R.E. and E.A.K. Cryo-EM and CLEM measurements were performed and analyzed by P.D.D. and E.A.K. The manuscript was written by E.A.K. and L.S.,

with input from P.D.D. and M.R.E. **Competing interests:** The authors declare that they have no competing interests. **Data and material availability:** Plasmids and strains used and created for this work can be obtained on request.

References

1. Komeili A, Li Z, Newman DK, Jensen GJ. 2006. Magnetosomes Are Cell Membrane Invaginations Organized by the Actin-Like Protein MamK. Science (80-) 311:242–246.
2. Cameron JC, Wilson SC, Bernstein SL, Kerfeld CA. 2013. Biogenesis of a bacterial organelle: The carboxysome assembly pathway. Cell 155:1131.
3. Jendrossek D, Pfeiffer D. 2014. New insights in the formation of polyhydroxyalkanoate granules (carbonosomes) and novel functions of poly(3-hydroxybutyrate). Environ Microbiol 16:2357–2373.
4. Qi Q, Rehm BHA. 2001. Polyhydroxybutyrate biosynthesis in Caulobacter crescentus: molecular characterization of the polyhydroxybutyrate synthase. Microbiology 147:3353–3358.
5. Anderson AJ, Dawes EA. 1990. Occurrence, metabolism, metabolic role, and industrial uses of bacterial polyhydroxyalkanoates. Microbiol Rev 54:450–472.
6. Beeby M, Cho M, Stubbe J, Jensen GJ. 2012. Growth and localization of polyhydroxybutyrate granules in ralstonia eutropha. J Bacteriol 194:1092–1099.
7. Griebel R, Smith Z, Merrick JM. 1968. Metabolism of Poly-β-hydroxybutyrate. I. Purification, Composition, and Properties of Native Poly-β-hydroxybutyrate Granules from Bacillus megaterium. Biochemistry 7:3676–3681.
8. Sznajder A, Pfeiffer D, Jendrossek D. 2015. Comparative proteome analysis reveals four novel polyhydroxybutyrate (PHB) granule-associated proteins in Ralstonia eutropha H16. Appl Environ Microbiol 81:1847–1858.
9. Bresan S, Sznajder A, Hauf W, Forchhammer K, Pfeiffer D, Jendrossek D. 2016. Polyhydroxyalkanoate (PHA) granules have no phospholipids. Sci Rep 6:1–13.
10. Pieper-Furst U, Madkour MH, Mayer F, Steinbuchel A. 1995. Identification of the region of a 14-kilodalton protein of Rhodococcus ruber that is responsible for the binding of this phasin to polyhydroxyalkanoic acid granules. J Bacteriol 177:2513–2523.
11. Wieczorek R, Steinbüchel A, Schmidt B. 1996. Occurrence of polyhydroxyalkanoic acid granule-associated proteins related to the Alcaligenes eutrophus H16 GA24 protein in other bacteria. FEMS Microbiol Lett 135:23–30.

12. Wieczorek R, Pries A, Steinbuchel A, Mayer F. 1995. Analysis of a 24-kilodalton protein associated with the polyhydroxyalkanoic acid granules in Alcaligenes eutrophus. J Bacteriol 177:2425–2435.
13. Neumann L, Spinozzi F, Sinibaldi R, Rustichelli F, Pötter M, Steinbüchel A. 2008. Binding of the major phasin, PhaP1, from Ralstonia eutropha H16 to poly(3-hydroxybutyrate) granules. J Bacteriol 190:2911–2919.
14. Mato A, Tarazona NA, Hidalgo A, Cruz A, Jiménez M, Pérez-Gil J, Prieto MA. 2019. Interfacial Activity of Phasin PhaF from Pseudomonas putida KT2440 at Hydrophobic-Hydrophilic Biointerfaces. Langmuir 35:678–686.
15. Zhao H, Wei H, Liu X, Yao Z, Xu M, Wei D, Wang J, Wang X, Chen GQ. 2016. Structural Insights on PHA Binding Protein PhaP from Aeromonas hydrophila. Sci Rep 6:1–13.
16. Liebergesell M, Sonomoto K, Madkour M, Mayer F, Steinbüchel A. 1994. Purification and Characterization of the Poly(Hydroxyalkanoic Acid) Synthase from Chromatium vinosum and Localization of the Enzyme at the Surface of Poly(Hydroxyalkanoic Acid) Granules. Eur J Biochem 226:71–80.
17. Wittenborn EC, Jost M, Wei Y, Stubbe JA, Drennan CL. 2016. Structure of the catalytic domain of the class I polyhydroxybutyrate synthase from Cupriavidus necator. J Biol Chem 291:25264–25277.
18. Arsad H, Chek MF, Samian MR, Hakoshima T, Sudesh K, Mori T, Kim S-Y. 2017. Structure of polyhydroxyalkanoate (PHA) synthase PhaC from Chromobacterium sp. USM2, producing biodegradable plastics. Sci Rep 7:1–15.
19. Gerngross TU, Martin DP. 1995. Enzyme-catalyzed synthesis of poly[(R)-(-)-3-hydroxybutyrate]: formation of macroscopic granules in vitro. Proc Natl Acad Sci 92:6279–6283.
20. Slater SC, Voige WH, Dennis DE. 1988. Cloning and expression in Escherichia coli of the Alcaligenes eutrophus H16 poly-β-hydroxybutyrate biosynthetic pathway. J Bacteriol 170:4431–4436.
21. Merrick JM, Doudoroff M. 1964. DEPOLYMERIZATION OF POLY-beta-HYDROXYBUTYRATE BY AN. J Bacteriol 88:60–71.
22. Lauzier C, Marchessault RH, Smith P, Chanzy H. 1992. Structural study of isolated poly(β-hydroxybutyrate) granules. Polymer (Guildf) 33:823–827.
23. Kawaguchi Y, Doi Y. 1990. Structure of native poly(3-hydroxybutyrate) granules characterized by X-ray diffraction. FEMS Microbiol Lett 70:151–155.
24. Horowitz DM, Sanders JKM. 1994. Amorphous, Biomimetic Granules of

Polyhydroxybutyrate: Preparation, Characterization, and Biological Implications. J Am Chem Soc 116:2695–2702.

25. Gebauer B, Jendrossek D. 2006. Assay of poly(3-hydroxybutyrate) depolymerase activity and product determination. Appl Environ Microbiol 72:6094–6100.
26. Jendrossek D, Knoke I, Habibian RB, Steinbüchel A, Schlegel HG. 1993. Degradation of poly(3-hydroxybutyrate), PHB, by bacteria and purification of a novel PHB depolymerase from Comamonas sp. J Environ Polym Degrad 1:53–63.
27. Saegusa H, Shiraki M, Kanai C, Saito T. 2001. Cloning of an intracellular Poly[D(-)-3-hydroxybutyrate] depolymerase gene from Ralstonia eutropha H16 and characterization of the gene product. J Bacteriol 183:94–100.
28. de Eugenio LI, García P, Luengo JM, Sanz JM, Román JS, García JL, Prieto MA. 2007. Biochemical evidence that phaZ gene encodes a specific intracellular medium chain length polyhydroxyalkanoate depolymerase in Pseudomonas putida KT2442. J Biol Chem 282:4951–4962.
29. Dufresne ER, Cabeen MT, Jacobs-Wagner C, Parry BR, Surovtsev IV, O'Hern CS. 2013. The Bacterial Cytoplasm Has Glass-like Properties and Is Fluidized by Metabolic Activity. Cell 156:183–194.
30. Ostle AG, Holt JG. 1982. Fluorescent Stain for Poly-3- Hydroxybutyrate. Appl Environ Microbiol 44:238–241.
31. Spiekermann P, Rehm BHA, Kalscheuer R, Baumeister D, Steinbüchel A. 1999. A sensitive, viable-colony staining method using Nile red for direct screening of bacteria that accumulate polyhydroxialkanoic acids and other lipit storage compounds. Arch Microbiol 171:73–80.
32. Juengert J, Bresan S, Jendrossek D. 2018. Determination of Polyhydroxybutyrate (PHB) Content in Ralstonia eutropha Using Gas Chromatography and Nile Red Staining. Bio-Protocol 8:1–15.
33. Sartori A, Gatz R, Beck F, Rigort A, Baumeister W, Plitzko JM. 2007. Correlative microscopy: Bridging the gap between fluorescence light microscopy and cryo-electron tomography. J Struct Biol 160:135–145.
34. Schwartz CL, Sarbash VI, Ataullakhanov FI, Mcintosh JR, Nicastro D. 2007. Cryo-fluorescence microscopy facilitates correlations between light and cryo-electron microscopy and reduces the rate of photobleaching. J Microsc 227:98–109.
35. Dahlberg PD, Saurabh S, Sartor AM, Wang J, Mitchell PG, Chiu W, Shapiro L, Moerner WE. 2020. Cryogenic single-molecule fluorescence annotations for electron tomography reveal in situ organization of key proteins in Caulobacter. Proc Natl Acad

Sci U S A 117:13937–13944.
36. Tarazona NA, Hernández-Arriaga AM, Kniewel R, Prieto MA. 2020. Phasin interactome reveals the interplay of PhaF with the polyhydroxyalkanoate transcriptional regulatory protein PhaD in Pseudomonas putida. Environ Microbiol 22:3922–3936.
37. Pfeiffer D, Jendrossek D. 2011. Interaction between poly(3-hydroxybutyrate) granule-associated proteins as revealed by two-hybrid analysis and identification of a new phasin in Ralstonia eutropha H16. Microbiology 157:2795–2807.
38. Buckley RM, Stubbe JA. 2015. Chemistry with an artificial primer of polyhydroxybutyrate synthase suggests a mechanism for chain termination. Biochemistry 54:2117–2125.
39. Maehara A, Taguchi S, Nishiyama T, Yamane T, Doi Y. 2002. A repressor protein, PhaR, regulates polyhydroxyalkanoate (PHA) synthesis via its direct interaction with PHA. J Bacteriol 184:3992–4002.
40. York GM, Stubbe J, Sinskeyl AJ. 2002. The ralstonia eutropha PhaR protein couples synthesis of the PhaP phasin to the presence of polyhydroxybutyrate in cells and promotes polyhydroxybutyrate production. J Bacteriol 184:59–66.
41. Chou ME, Yang MK. 2010. Analyses of binding sequences of the PhaR protein of Rhodobacter sphaeroides FJ1. FEMS Microbiol Lett 302:138–143.
42. Pötter M, Müller H, Steinbüchel A. 2005. Influence of homologous phasins (PhaP) on PHA accumulation and regulation of their expression by the transcriptional repressor PhaR in Ralstonia eutropha H16. Microbiology 151:825–833.
43. Yamada M, Takahashi S, Okahata Y, Doi Y, Numata K. 2013. Monitoring and kinetic analysis of the molecular interactions by which a repressor protein, PhaR, binds to target DNAs and poly[(R)-3-hydroxybutyrate]. AMB Express 3:3–9.
44. Buckley RM. 2013. The role of the phasin PhaP in promoting polyhydroxybutyrate (PHB) granule formation in Caulobacter crescentus.
45. Grant CR, Wan J, Komeili A. 2018. Organelle Formation in Bacteria and Archaea. Annu Rev Cell Dev Biol 34:217–238.
46. Blakemore R. 1974. Magnetotactic Bacteria. Science (80-) 190:377–379.
47. Scheffel A, Gruska M, Faivre D, Linaroudis A, Plitzko JM, Schüler D. 2006. An acidic protein aligns magnetosomes along a filamentous structure in magnetotactic bacteria. Nature 440:110–114.
48. Uebe R, Keren-Khadmy N, Zeytuni N, Katzmann E, Navon Y, Davidov G, Bitton R, Plitzko JM, Schüler D, Zarivach R. 2018. The dual role of MamB in magnetosome membrane assembly and magnetite biomineralization. Mol Microbiol 107:542–557.

49. Raschdorf O, Forstner Y, Kolinko I, Uebe R, Plitzko JM, Schüler D. 2016. Genetic and Ultrastructural Analysis Reveals the Key Players and Initial Steps of Bacterial Magnetosome Membrane Biogenesis. PLoS Genet 12:1–23.
50. Hill NC, Tay JW, Altus S, Bortz DM, Cameron JC. 2020. Life cycle of a cyanobacterial carboxysome. Sci Adv 6:1–8.
51. Ren Q, Roo G De, Ruth K, Witholt B, Zinn M. 2009. Simultaneous Accumulation and Degradation of Polyhydroxyalkanoates : Futile Cycle or Clever Regulation ? 916–922.
52. Prieto A, Escapa IF, Martínez V, Dinjaski N, Herencias C, de la Peña F, Tarazona N, Revelles O. 2016. A holistic view of polyhydroxyalkanoate metabolism in Pseudomonas putida. Environ Microbiol 18:341–357.
53. Doi Y, Segawa A, Kawaguchi Y, Kunioka M. 1990. Cyclic nature of poly(3-hydroxyalkanoate) metabolism in Alcaligenes eutrophus. FEMS Microbiol Lett 165–169.
54. Taidi B, Mansfield DA, Anderson AJ. 1995. Turnover of poly(3-hydroxybutyrate) (PHB) and its influence on the molecular mass of the polymer accumulated by Alcaligenes eutrophus during batch culture. FEMS Microbiol Lett 129:201–205.
55. Jossek R, Steinbüchel A. 1998. In vitro synthesis of poly(3-hydroxybutyric acid) by using an enzymatic coenzyme A recycling system. FEMS Microbiol Lett 168:319–324.
56. Juengert JR, Patterson C, Jendrossek D. 2018. Poly(3-Hydroxybutyrate) (PHB) Polymerase PhaC1 and PHB Depolymerase PhaZa1 of Ralstonia eutropha Are Phosphorylated In Vivo. Appl Environ Microbiol 84:e00604-18.
57. Bresan S, Jendrossek D. 2017. New Insights into PhaM-PhaC-Mediated Localization of Polyhydroxybutyrate Granules in Ralstonia eutropha H16. Appl Environ Microbiol 83:1–14.
58. Pfeiffer D, Jendrossek D. 2014. PhaM Is the Physiological Activator of Poly(3-Hydroxybutyrate) (PHB) Synthase (PhaC1) in Ralstonia eutropha. Appl Environ Microbiol 80:555–563.
59. Pfeiffer D, Wahl A, Jendrossek D. 2011. Identification of a multifunctional protein, PhaM, that determines number, surface to volume ratio, subcellular localization and distribution to daughter cells of poly(3-hydroxybutyrate), PHB, granules in Ralstonia eutropha H16. Mol Microbiol 82:936–951.
60. Thanbichler M, Iniesta AA, Shapiro L. 2007. A comprehensive set of plasmids for vanillate - And xylose-inducible gene expression in Caulobacter crescentus. Nucleic Acids Res 35.
61. Mastronarde DN. 2003. SerialEM: A program for automated tilt series acquisition on

Tecnai microscopes using prediction of specimen position. Microsc Microanal 9:1182–1183.

62. Dahlberg PD, Sartor AM, Wang J, Saurabh S, Shapiro L, Moerner WE. 2018. Identification of PAmKate as a Red Photoactivatable Fluorescent Protein for Cryogenic Super-Resolution Imaging. J Am Chem Soc 140:12310–12313.
63. Dahlberg PD, Perez D, Hecksel CW, Chiu W, Moerner WE. 2022. Metallic support films reduce optical heating in cryogenic correlative light and electron tomography. J Struct Biol 214:107901.
64. Kremer JR, Mastronarde DN, McIntosh JR. 1996. Computer visualization of three-dimensional image data using IMOD. J Struct Biol 116:71–76.
65. Livak KJ, Schmittgen TD. 2001. Analysis of relative gene expression data using real-time quantitative PCR and the 2-ΔΔCT method. Methods 25:402–408.
66. Saurabh S, Chong TN, Bayas C, Dahlberg PD, Cartwright HN, Moerner WE, Shapiro L. 2022. ATP-responsive biomolecular condensates tune bacterial kinase signaling. Sci Adv 8:1–17.

Figure 1

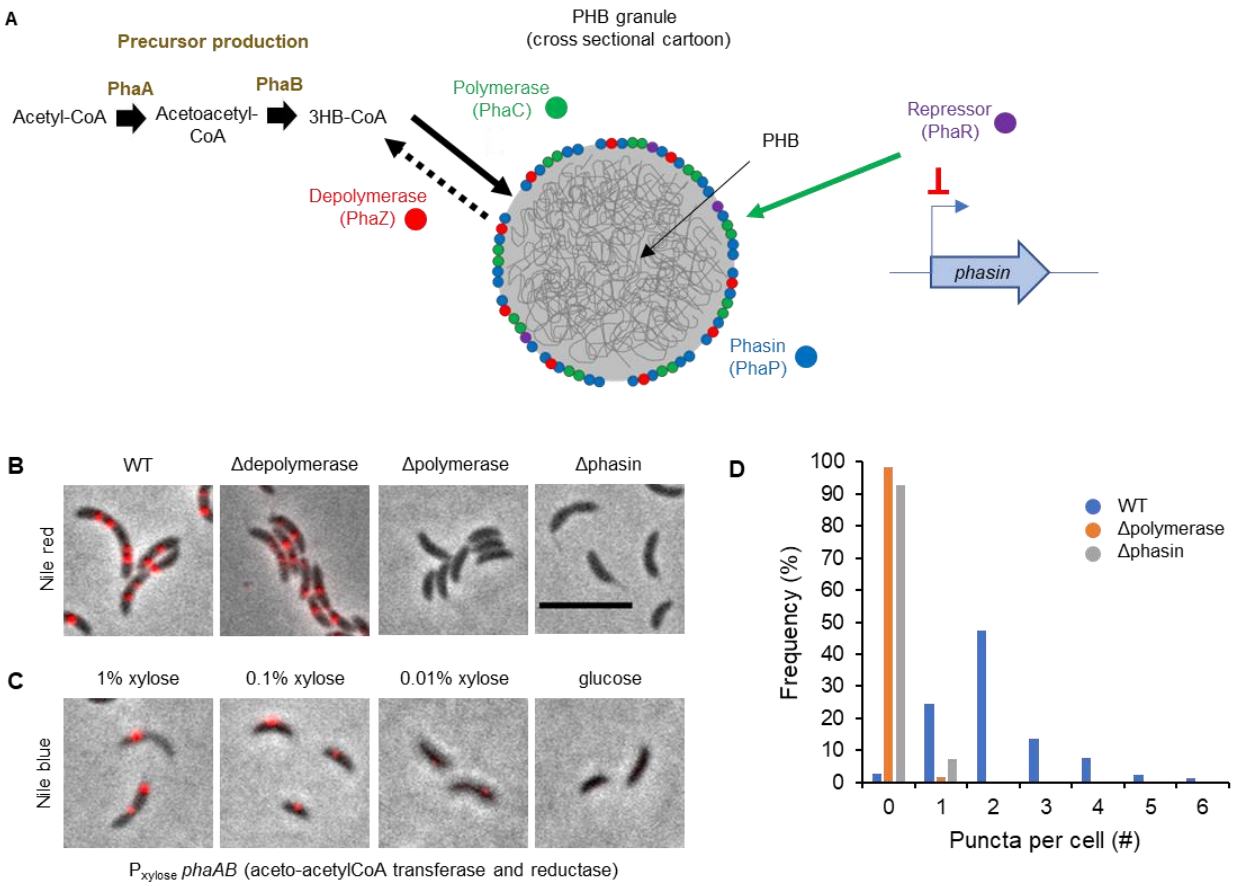

Figure 1. WT PHB granule formation requires both active polymerase and phasin

A) Schematic of PHB granule organization. A PHB granule consists mainly of water-insoluble PHB, with granule associated proteins on its surface (7). PHB is synthesized by the polymerase PhaC using the 3HB-CoA precursor. This precursor is generated from acetyl-CoA by PhaA and PhaB (20). PHB is consumed by the depolymerase PhaZ, possibly with uncharged CoA as an acceptor for released monomers. Both PhaC and PhaZ are associated with the granule, while PhaA and PhaB are not (8). Another abundant granule associated protein is phasin (PhaP). Its expression is regulated by the transcriptional repressor PhaR, which itself is sequestered to the granule upon PHB synthesis (40, 41). **B)** Deletion of either polymerase PhaC or phasin PhaP results in a loss of nile-red stained granules. Overlay images of phase contrast and nile-red fluorescence. Cells are stained in PBS with 1 μM nile red for 20 minutes. Strains used are WT NA1000, Δ*phaZ* (CCNA_00250::*tetR*), Δ*phaC* (CCNA_01444::*rifR*) and Δ*phaP* (CCNA_02242::*catR*). Scale bar is 5 μm. **C)** Reducing precursor availability results in a reduction in nile blue signal and loss of stained granules. Overlay images of phase contrast and nile blue fluorescence. Cells are stained M2G with 10 μM nile blue for 20 minutes. The strain contains a xylose inducible promoter at the start of the CCNA_00544-00545 (phaA-phaB) operon. An overnight culture in minimal medium was subcultured for 5 hours in the presence of increasing concentration of xylose. **D)** Quantification of (B), at least 600 cells were analyzed per strain.

Figure 2

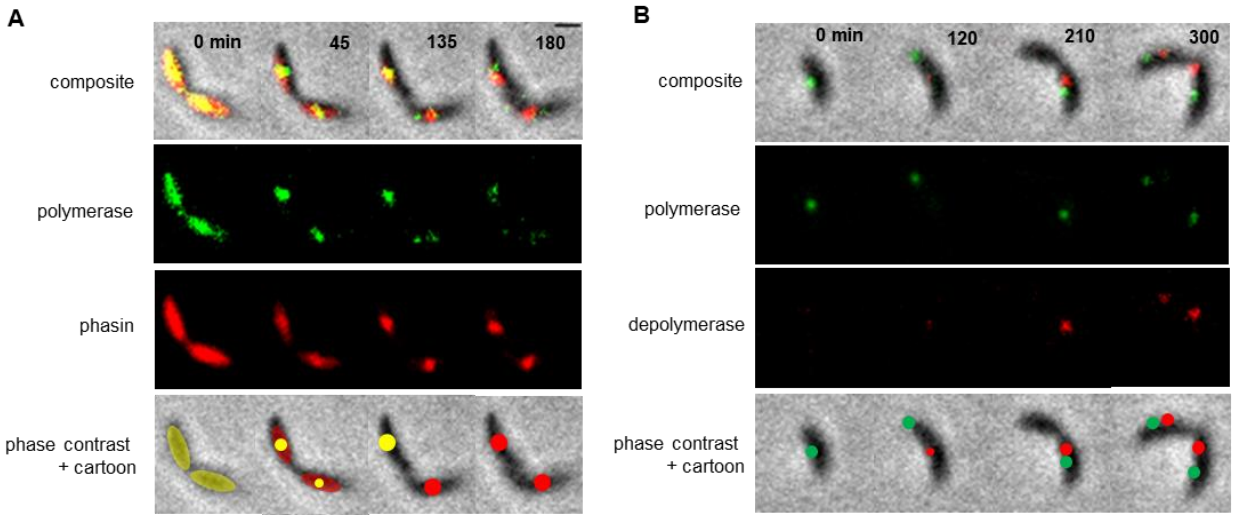

Figure 2. Polymerase localization precedes phasin and depolymerase accumulation

A) Timelapse of granule formation. Cells expressing both natively tagged polymerase-GFP and phasin-mCherry were starved of glucose for 24hrs in M2 (0 min), after which they were imaged upon reintroduction of glucose at the times shown. The cartoon depicts co-localization of GFP and mCherry signal as yellow. Scale bar is 1 μm. **B)** Timelapse of granule formation of cells expressing both natively tagged polymerase-GFP and depolymerase-mCherry.

Figure 3

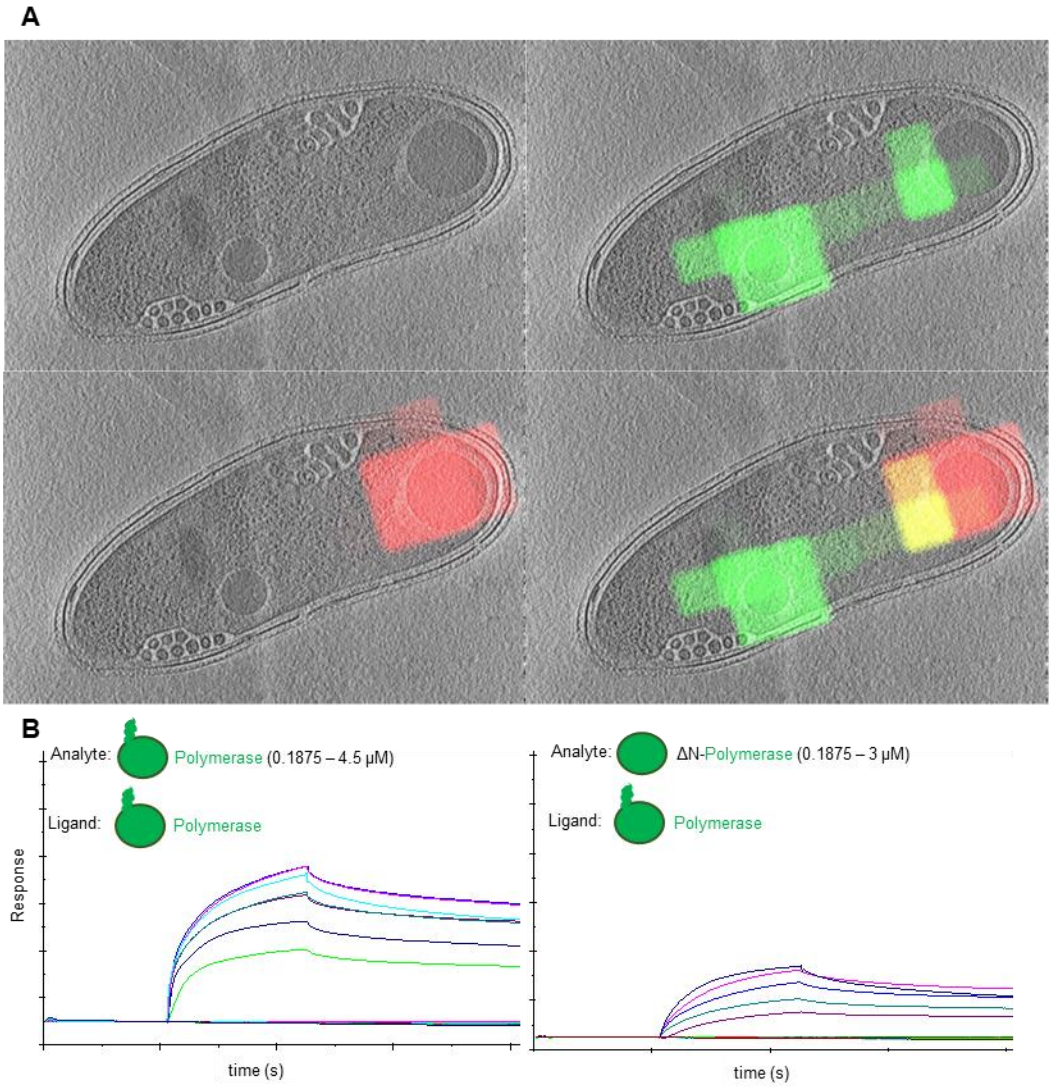

Figure 3. Granule maturation shown by cryo-CLEM and polymerase self-interaction shown by SPR

A) Example of a cell expressing polymerase-GFP and PHB granule stained with nile red. A tomographic slice from a 3D reconstruction (top left) shows 2 granules in this cell. Polymerase-GFP signal is co-localizing with both these granules (top right). However, only the larger granule stains for nile-red (bottom left). An overlay image shows the co-localization of polymerase-GFP and nile-red in yellow in the larger granule (bottom right). **B)** Purified polymerase was tested on self-interaction *in vitro* using surface plasmon resonance. Polymerase was immobilized on the surface using amine crosslinking as ligand, and either full-length polymerase or the N-terminal mutant were flown over as analyte.

Figure 4

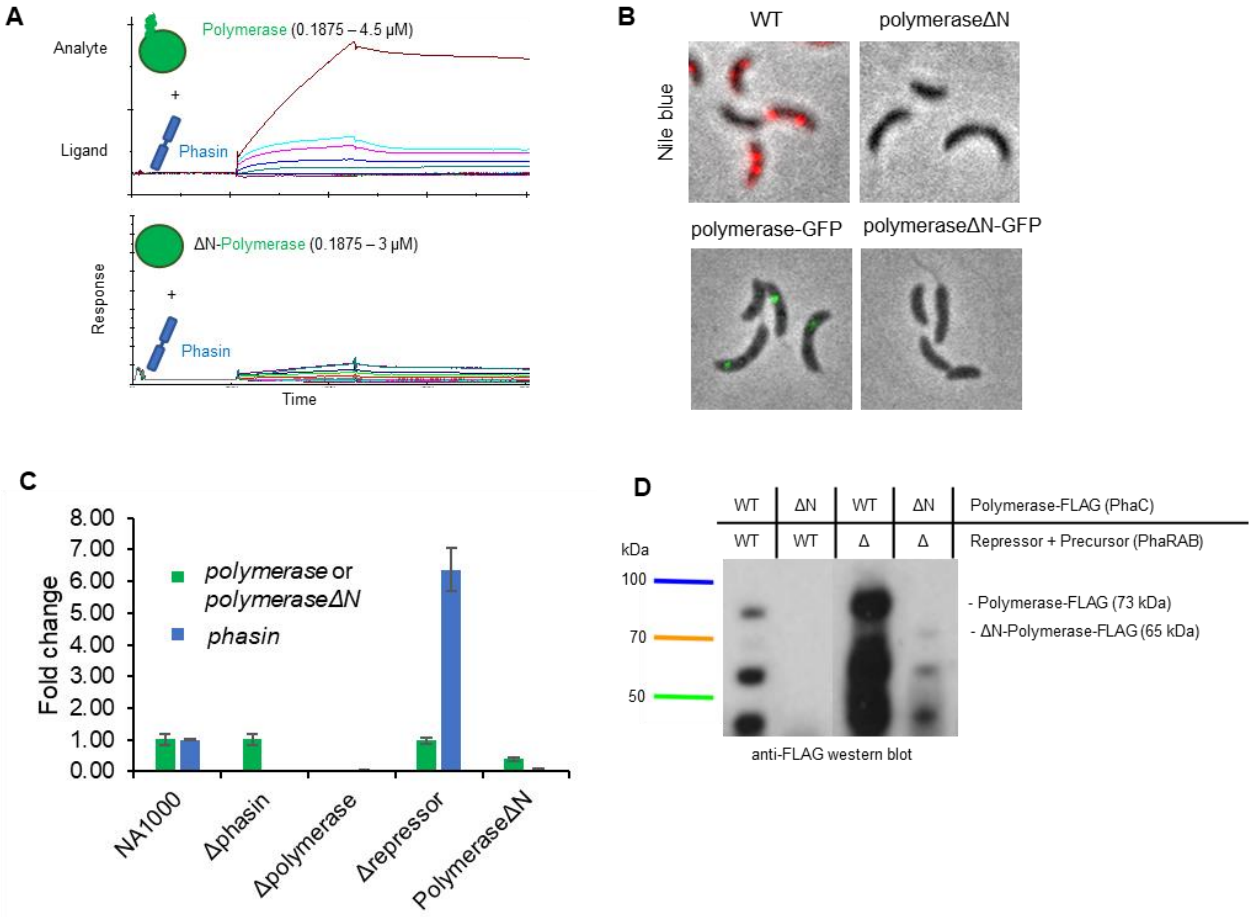

Figure 4. Phasin and Polymerase interact directly through polymerase N-terminus. Polymerase N-terminus is essential for *in vivo* granule formation
A) Polymerase binds immobilized phasin, but polymeraseΔN does not. Surface plasmon resonance response curves of increasing concentrations of either polymerase (top) or polymeraseΔN (bottom) flown over surface immobilized phasin. **B)** PolymeraseΔN cells have a large reduction in Nile blue stained granules. Fluorescently labeled PolymeraseΔN fails to localize. Overlay images of phase contrast and nile blue fluorescent signal. Localization of full length or mutant polymerase. Overlay images of phase contrast and GFP fluorescent signal. **C)** qPCR determining transcription of *polymerase* (CCNA_01444), *polymeraseΔN* or *phasin* (CCNA_02242) in different backgrounds. WT (N1000), Δ*phasin* (CCNA_02242*::catR*), Δ*polymerase* (CCNA_01444*::rifR*), Δ*repressor* (Δ*CCNA_00543*) and *polymeraseΔN* (*CCNA_01444Δ1-255bp*). Expression of *rho* was used as an endogenous control and fold change was determined by relative quantification (ΔΔCq method). **D)** Western Blot of FLAG-tagged polymerase (full length or ΔN) expressed from the native locus shows an increased detection of protein in cells lacking precursor production.